2005 American Control Conference
June 8-10, 2005. Portland, OR, USA

Model Based Control of a Multidimensional Positioning System - A Comparison of Controller Designs with Experimental Validation

Elizabeth Villota, Suhada Jayasuriya and Murray Kerr

Abstract— **The present study investigates the controlled behavior of a Multidimensional Positional System (MPS), under the application of model based control techniques (lead-lag, LQR, LQG, LQG-LTR, $\mathcal{H}_\infty$, μ-synthesis and QFT). The MPS consists of a magnetically levitated system capable of six degree-of-freedom micro and nano positioning using three novel permanent-magnet linear motors. Each motor generates a vertical force for suspension against gravity and a horizontal force for drive. Particular attention is given to the design, analysis and simulation of the control laws that guarantee tracking performance under modeled uncertainties. Closed loop identification is used to derive bounds of the variations in magnitude of the experimental data and mathematical models. Results obtained from numerical simulations are presented and judged with respect to the performance and stability achieved and the work needed to perform the designs. Laboratory experiments indicate partial success in the implementation of the designed control systems. Hence limited experimental results are presented to validate the performance of the control systems.**

I. INTRODUCTION

A Multidimensional Positional System (MPS) has been designed and assembled in the Mechatronics Laboratory at Texas A&M University for inhouse research in multi degree-of-freedom (DOF) positioning of a single magnetically levitated moving part (platen) at micro and nano scales, and for experimental testing of controller designs and identification algorithms. The working principle of the MPS is a linear motor capable of providing forces for both suspension and translation without contact. Reference [2] gives a detailed description of the facility.

Positional control for the MPS consists of six DOF control of the platen in the presence of external disturbances and model uncertainties. The platen has attached three windings (coils) on its bottom surface and is levitated above a two-dimensional superimposed concentrated-field magnet matrix (stator). See schematic illustration in Fig. 1.

The primary assumption in the present study is that a dynamical model, sufficient for control design, can be obtained from first principles and experimental tests. The platen is modeled as a rigid body. The motion of a rigid body undergoing six DOF is nonlinear. Hence the linear, time invariant motion about an equilibrium point is considered.

The control techniques used for the design of the feedback controllers are lead-lag, LQR, LQG, LQG-LTR, $\mathcal{H}_\infty$, μ-synthesis and QFT. The control systems are to be designed such that the MPS tracks simultaneous position and rotation commands for all the six DOF. Similar command following and disturbance rejection specifications in the frequency and time domain are posed for all designs. For design purposes only the $\mathcal{H}_\infty$, μ-synthesis and QFT control techniques explicitly incorporate the system uncertainty in the controller design. This uncertainty ideally accounts for the system dynamics not captured in the analytical model.

Using numerical simulations the merits of each controller are analyzed based on the quality of the control system in nominal operation (tracking, disturbance rejection and stability) and under the inclusion of uncertainty (performance and stability robustness) via $\mathcal{H}_\infty$ (μ) constraints on certain frequency weighted transfer matrices. The effort involved in the controller design is also considered (note that no tuning is permitted). From the laboratory experiments shown, a comparison is performed in terms of the agreement, or lack thereof, between simulations and experimental results.

The remainder of this paper is organized as follows. A brief description of the modeling issues and the linearized dynamics is presented in Section 2. The main differences among the control design approaches are explained in Section 3. Section 4 presents the numerical results, along with limited experimental results. The latter verifies that control objectives are achievable. Finally the results are discussed and future work is proposed.

II. MPS MATHEMATICAL MODEL

Figure 1 depicts the MPS [2]. The MPS is formed by the stator and the platen. On the stator there is attached a two-dimensional superimposed concentrated-field magnet

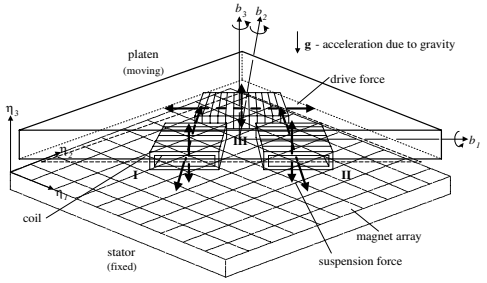

Fig. 1. 6 degree-of-freedom positioner.

This work was supported by Advanced Technology Program, Texas Higher Education Coordinating Board.

Elizabeth Villota is a graduate student in the Department of Mechanical Engineering, Texas A&M University, College Station, TX 77845, USA elvillota@tamu.edu

Suhada Jayasuriya is Kotzebue Professor in the Department of Mechanical Engineering, Texas A&M University, College Station, TX 77845, USA sjayasuriya@tamu.edu

Murray Kerr is a Postdoctoral Student in the Department of Mechanical Engineering, Texas A&M University, College Station, TX 77845, USA mkerr@tamu.edu

matrix. On the bottom surface of the platen are attached the coils that energize the actuation of the system. The currents pass through the coils and generate forces and torques on the center of mass of the platen due to the interaction between the current distribution and the magnet array [6]. A set of orthogonal (b_1, b_2, b_3) body fixed axes defines the motion of the platen with respect to the inertial frame (stator). The platen coordinate system is initially aligned to the (η_1, η_2, η_3) coordinate system fixed to the stator. The platen is modeled as a rigid body and has six DOF. To avoid thermal problems, the platen is suspended by means of air bearings. The air bearings are modeled as three linear springs.

The translational acceleration of the platen, $\vec{v}$, in inertial coordinates, can be written as

$$\dot{\vec{v}} = -\frac{1}{M}\left[\underline{K}_t\vec{x} + \vec{g} - \underline{C}^T\vec{F}\right], \tag{1}$$

where M is the mass of the platen, $\underline{K}_t = \text{diag}([0, 0, k_{x_3}])$ is the linear spring constant matrix, $\vec{x}$ is the linear position vector of the platen centroid, $\vec{v}$ is the linear velocity vector, $\vec{g} = [0, 0, g]$ with g being the acceleration of the gravity, $\underline{C}$ is the transformation matrix from the inertial to body coordinates and $\vec{F}$ is the vector of magnetic forces. The magnetic forces $\vec{F}_j$, j=[I,II,III] (related to each coil) depend on the instantaneous centroid location of the platen, $\vec{x} = [x_1, x_2, x_3]^T$, and the current applied to the coils.

The angular acceleration of the platen, $\dot{\vec{\omega}}$, in body coordinates, can be written as

$$\dot{\vec{\omega}} = -\underline{I}^i\left[\underline{K}_r\vec{\beta} + \vec{\omega}\times\underline{I}\cdot\vec{\omega} - \vec{\tau}\right], \tag{2}$$

where $\vec{\beta}$ denotes the rotational position vector of the platen centroid, $\vec{\omega}$ is the angular velocity vector, $\underline{I}^i$ denotes the inverse of the inertia tensor $\underline{I}$, $\underline{K}_r = \text{diag}([k_{\beta_1}, k_{\beta_2}, 0])$ is the rotational spring constant matrix and $\vec{\tau} = \sum_{j=\text{I}}^{\text{III}}\vec{r}_j\times\vec{F}_j$ is the vector of control input torques produced by the magnetic forces, where $\vec{r}_j$, $j = [\text{I}, \text{II}, \text{III}]$, denote the position of each coil centroid with respect to the platen centroid.

The magnetic forces, defined in terms of the quadrature and direct currents i_q and i_d respectively, are as follows

$$\begin{bmatrix} F_{ji} \\ F_{j3} \end{bmatrix} = \frac{1}{2}\mu_o M_o \eta_o N_m G\mathbf{e}^{-\gamma_1 x_3}\begin{bmatrix} i_{qj} \\ i_{dj} \end{bmatrix}, \tag{3}$$

with $i = [1, 2]$, as in [7]. The quadrature and direct currents can also be considered for analysis and synthesis of the controllers. The MPS parameters have the following values: the magnet remanence is $\mu_o M_o = 0.71$T, the winding turn density is $\eta_o = 3.5246\times10^6$turns/m^2, the number of active magnet pitches is $N_m = 2$, the pitch is $l = 51.2$mm, the fundamental wave number is $\gamma_1 = 2\pi/l = 123.25\text{m}^{-3}$ and the motor geometry constant is $G = 1.0722\times10^{-5}\text{m}^3$. The platen mass is 5.91kg. The elements of the spring constant matrices are $k_{\beta_1} = 1.065\times10^4$N/kgm, $k_{\beta_2} = 1.131\times10^4$ N/kgm and $k_{x_3} = 10^6$N/kg. The inertia tensor is

$$\underline{I} = \begin{bmatrix} 0.0357 & -0.0012 & -0.0008 \\ -0.0012 & 0.0261 & 0.0003 \\ -0.0008 & 0.0003 & 0.0561 \end{bmatrix}\ \text{kgm}^2. \tag{4}$$

The resultant model is nonlinear and is of the form

$$\dot{\eta} = g(\eta, u) = f(\eta, i), \tag{5}$$

where $\eta = [\,v_1, v_2, v_3, x_1, x_2, x_3, \omega_1, \omega_2, \omega_3, \beta_1, \beta_2, \beta_3\,]^T$ is the state vector and $u = [\,F_1, F_2, F_3, \tau_1, \tau_2, \tau_3\,]^T$ and $i = [\,i_{q\text{I}}, i_{q\text{II}}, i_{q\text{III}}, i_{d\text{I}}, i_{d\text{II}}, i_{d\text{III}}\,]^T$ are the control input vectors.

A. Linearized Model

The equilibrium state η_o corresponds to the body frame being collinear with the inertial frame. Hence

$$\eta_o = [\ 0, 0, 0, 0, 0, 2.324\text{mm}, 0, 0, 0, 0, 0, 0\ ]^T \tag{6}$$

and the linearized perturbed motion about the equilibrium can be given by

$$\delta\dot{\eta} = A\,\delta\eta + B_u\delta u = A\,\delta\eta + B_i\delta i. \tag{7}$$

The linearized analytical models are used in the design of the multiple-input multiple-output (MIMO) controllers. Due to the diagonal dominance of the inertia tensor (4), the linear model corresponding to forces and torques as control inputs can be decoupled and subsequently a decentralized single-input single-output (SISO) control system design is feasible. For implementation purposes, it was useful to work with two models in the design. These models represent the horizontal[1] (unstable) and vertical[2] (stable) motions.

B. Actuation and Sensing System

The control input consists of the direct and quadrature currents, related to the phase currents, going into the three coils. The current into the coils generates a magnetic field which produces a net force and torque on the suspended platen. The resulting motion is sensed by laser interferometers and optical sensors.

The laser interferometers give relative position information of the full horizontal motion with a 0.6nm resolution at 10MHz update rate and for velocity data of up to 1m/s. The optical sensors give voltage information for the vertical motion (only position) with a resolution of 15nm and for 100μm of measurement range.

The output equation is defined as

$$y = C\,\delta\eta, \tag{8}$$

where y is the vector of physical variables sensed and C is the output matrix.

C. Model Validation and Identification of the MPS

System identification is required to verify that the analytical model is valid for controller design. Open loop tests cannot be performed due to the unstable nature of the MPS. Subsequently, identification of the experimental system is carried on the closed loop system with a lead-lag (decentralized) controller under the consideration that the linear model is decoupled. The joint input-output approach, [10],

[1]Horizontal motion: x_1, x_2, β_3, v_1, v_2 and ω_3

[2]Vertical motion: β_1, β_2, x_3, ω_1, ω_2 and v_3.

was used for each DOF of the closed loop. The input test signal, r reference, consisted of a zero mean, white noise random signal with standard deviation of 0.01 and 0.05μm for the horizontal and vertical motion, respectively. The total time of the excitation signal is 2s at a 5kHz sampling rate. Observing the frequency response, Fig. 2, significant mismatch between the analytical and experimental models is apparent, especially at low and high frequencies. The mismatch at low frequencies is likely because the excitation signals did not contain much energy over that frequency range. At high frequencies the mismatch is due to the unmodeled dynamics. Notably, for the horizontal motion, the experimental models present resonances at around 90Hz.

D. Uncertainty Model

The uncertainty models are determined by the discrepancy between the derived, simple analytical uncoupled model and the experimental model, with the analytical coupled model serving as the nominal model for controller design. Knowing that for systems such the MPS the main source of errors are the high frequency dynamics, additive uncertainty models are constructed as shown in Fig. 2. These high frequency dynamics may be caused by nonlinearities, mechanical-electrical couplings and environmental noises. At low frequencies uncertainty is not as important since high gain will be employed at those frequencies. Figure 3 shows the schematic of the closed loop system where the uncertainty model maps force and torque inputs to physical outputs.

III. CONTROLLER DESIGN

The main objective of the control systems is to stabilize the platen dynamics and track[3] a command signal about the equilibrium state with 2% steady state error. The challenging aspect of the design is to guarantee a specific tracking performance in spite of imperfect knowledge of the experimental system whilst accommodating the physical limitations (saturation, sampling, etc). The controllers are also designed to attenuate disturbances in the low frequency band from 0 to 30Hz and to have less than 30% overshoot with a rise time (to within 80% of the final value) of less than 0.1s for a step change in the reference input, for all axes. For planar movement, the dynamic performance objectives include hundreds of millimeters traveling with a maximum speed capability of 1m/s.

In the LQG-LTR [1], lead-lag [5], LQR [4] and LQG [4] designs zero steady state error for step inputs is achieved by inserting an integrating action. In the lead-lag design, the SISO diagonal controller elements are designed independently and have a phase margin of 40^o. The total order of the controller is 12 and the loop bandwidth is 30Hz and 140Hz for the horizontal and vertical motion, respectively. For the LQR and LQG designs, information available from the experimental models is used to choose the weighting matrices. The total order of the LQG-LTR controller for each motion is 12 (horizontal and vertical), the loop bandwidth is 30Hz for the horizontal motion and 100Hz for the vertical one. For the $\mathcal{H}_\infty$ and μ-synthesis designs [12], the uncertainty model is explicitly incorporated in the design. The order of the controllers is reduced to 15, at most, for each motion. The loop bandwidth is 30Hz for the horizontal motion and 110Hz for the vertical one. In the QFT design [11] (a two DOF design) the prefilter is designed to enforce closed loop tracking requirements, increasing the order of the controller. The total QFT controller order is 36.

[3] An implicit performance requirement is constant disturbance rejection.

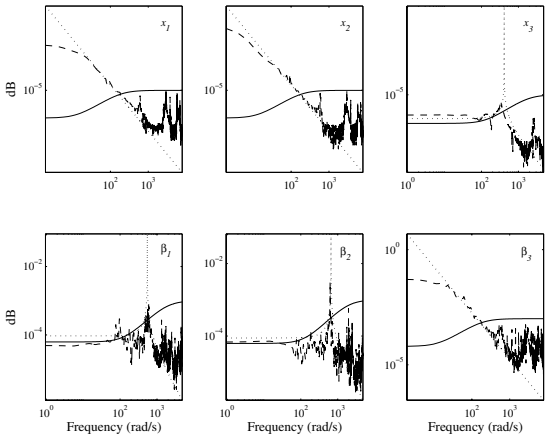

Fig. 2. Comparison of the analytical model (dotted) and the identified model (dashed). Additive uncertainty model (solid line).

IV. RESULTS

This section presents the numerical simulations of the controlled MPS response and limited experimental results[4]. The quality of the controllers is analyzed in both the frequency and time domain.

A. Numerical Simulations Comparison

This section compares the properties of the designed control systems. Notably, there doesn't exist a general method to compare the designed control systems. However, the use of the $\mathcal{H}_\infty$ norm or μ scalar of the frequency weighted transfer functions, as it is done in the $\mathcal{H}_\infty$ and μ-synthe-

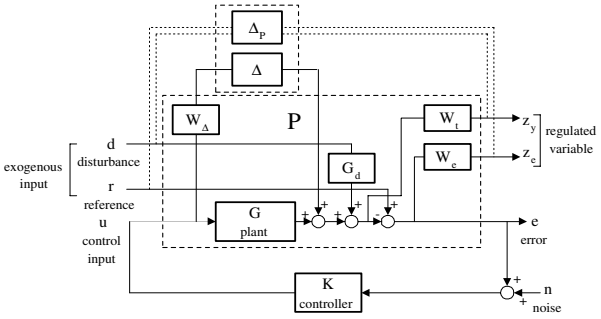

Fig. 3. Closed loop system for comparison.

[4] All the results and simulations are computed using the Control, μ-synthesis and QFT Matlab Toolboxes.

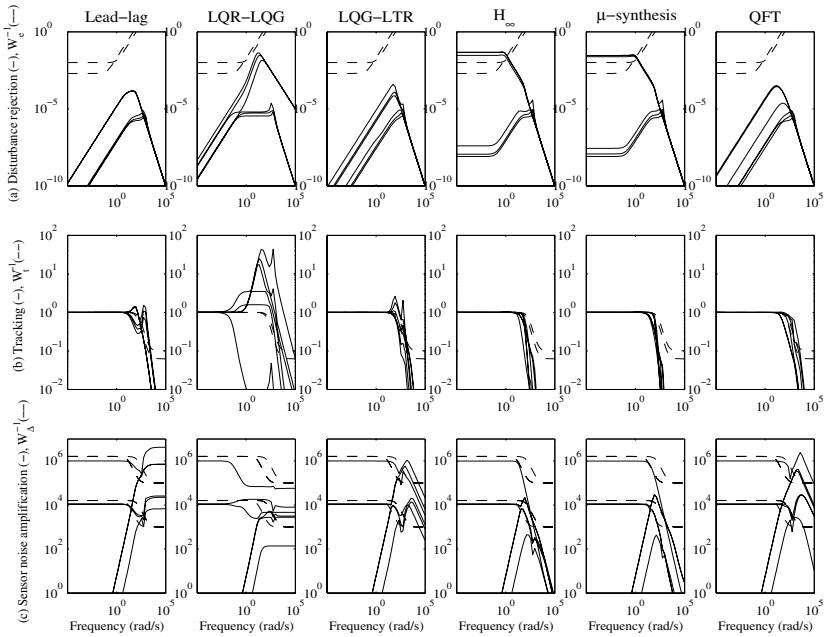

Fig. 4. Singular values: (a) Disturbance rejection, (b) Tracking and (c) Sensor noise amplification (Δ=0).

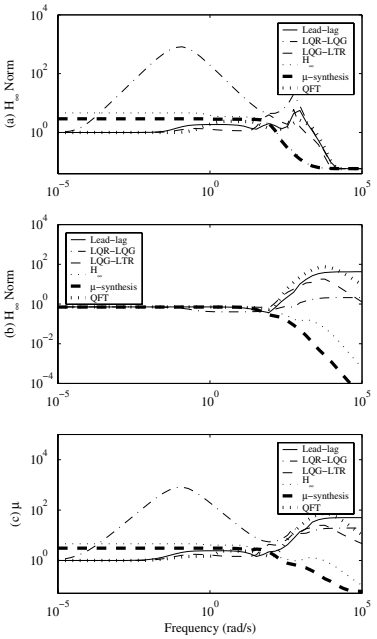

Fig. 5. (a) Nominal Performance, (b) Robust Stability and (c) Robust Performance.

sis designs, proved to be useful for comparing the performance and stability of the designs. In the following, the $\mathcal{H}_\infty$ norm and μ scalar are employed to facilitate comparison and all conclusions are given with respect to the values of the norms (or scalars) associated to the weighted transfer functions (see Fig. 3). The weighting functions employed for the $\mathcal{H}_\infty$ and μ-synthesis designs are also used when comparing the designs.

1) Frequency Domain Response: Nominal performance, robust stability and robust performance are investigated.

Nominal Performance (NP). The requirements for NP ($\Delta = 0$) are $\|W_e S G_d\|_\infty \leq 1$ for disturbance rejection and $\|W_t T\|_\infty \leq 1$ for reference tracking. S and T are the sensitivity and complementary sensitivity function respectively.

From Fig. 4(a) all the controllers present good disturbance rejection properties, except the $\mathcal{H}_\infty$ and μ-synthesis controllers which violate the disturbance rejection condition at very low frequencies. Whilst minor in the case of QFT, aside from $\mathcal{H}_\infty$ and μ-synthesis, the other controllers violate the tracking condition (see Fig. 4(b)).

Figure 5(a) shows that no controller presents an $\mathcal{H}_\infty$ norm less than one for the NP weighted transfer matrix. This is not surprising as previous plots (Fig. 4(a)-(b)) show that none of the controllers satisfy both performance conditions simultaneously. The worst performance is presented by the LQR-LQG controller that possesses the highest peaks for tracking. The violation of the disturbance rejection by the $\mathcal{H}_\infty$ and μ-synthesis controllers is shown at low frequencies where the $\mathcal{H}_\infty$ norms are 4.5 and 3.0, respectively. For the other controllers, good tracking of signals at low frequencies ($\mathcal{H}_\infty$ norm about 1) and degraded behavior near the crossover frequencies ($\mathcal{H}_\infty$ norm increased by a factor of up to 5) can be seen in the plot. The peaks at intermediate frequencies reflect the peaks the controllers present for tracking. Among the controllers, the QFT controller achieves the best NP.

Robust Stability (RS). The consideration of additive uncertainty enforces the condition $\|W_\Delta K S\|_\infty \leq 1$ for RS.

Figure 5(b) shows that only the $\mathcal{H}_\infty$ and μ-synthesis controllers achieve RS. This is to be expected as these controllers were designed considering the weighted uncertainty model. For the $\mathcal{H}_\infty$ and μ-synthesis controllers, the weighted sensor noise amplification matrix, $W_\Delta K S$, present a peak of 0.7. This implies that for diagonal perturbations smaller than 1/0.7 the closed-loop system remains stable. For the other controllers it can be said that they are more sensitive to diagonal perturbations. Specifically, the closed loop system for the QFT controller becomes unstable for the smallest diagonal perturbations. The LQR-LQG controller, which presented the worst NP, has better RS properties than the other controllers, except for the $\mathcal{H}_\infty$ and μ-synthesis controllers. In particular, the RS condition is violated by all the controllers except $\mathcal{H}_\infty$ and μ-synthesis in the high frequency region. This also can be visualized in Fig. 4(c) where at high frequencies the singular values of KS are not below the inverse of W_Δ.

Robust Performance (RP). The closed loop system achieves RP if the closed loop system is internally stable for all the plants $G_\Delta = G + W_\Delta \Delta$ ($\|\Delta\|_\infty \leq 1$) and the following performance objectives are satisfied: $\|W_e \frac{I}{I+G_\Delta K} G_d\|_\infty \leq 1$ and $\|W_t \frac{G_\Delta K}{I+G_\Delta K}\|_\infty \leq 1$.

Figures 5(a)-(b) show that no controller satisfies NP and

RS conditions simultaneously, hence RP is not achievable, as confirmed in Fig. 5(c). Observing the peaks attained for each controller, the μ scalar of the diagonal perturbations that cause deterioration of performance can be calculated. Under this consideration, the $\mathcal{H}_\infty$ and μ-synthesis controllers present better RP properties. This is not unexpected as these controllers considered the performance weighting functions in the design. Figure 5(c) also shows that the NP characteristics of the controlled systems are maintained at low frequencies, while at high frequencies the RS characteristics dominate.

It is worth recalling that the values obtained for the NP, RS and RP are only valid with respect to the performance and stability definitions, and the model of uncertainty considered in the design. If the family of plants considered in the design of the $\mathcal{H}_\infty$ and μ-synthesis controllers, and in the comparison, is erroneous, the resultant RS and RP can be not reliable.

2) Time Domain Response: Figure 6 shows the step responses of the six position variables of the platen, for the nominal model. In general, all controllers present fast tracking of the steps. As stated in the previous section, the QFT controller is the one that gives the best performance.

The large peaks in the frequency plots for LQR-LQG tracking are reflected in the large overshoot and slow response presented in the corresponding step response. The $\mathcal{H}_\infty$, μ-synthesis and QFT controllers present well damped responses while the lead-lag and LQG-LTR controllers present overshoot for the horizontal motion responses.

B. Preliminary Experimental Results

The lead-lag, LQR-LQG, LQG-LTR and $\mathcal{H}_\infty$[5] controllers have been implemented and tested with a sampling rate of 5kHz. The performance of each control system is compared with respect to the numerical results. Notably, the MIMO $\mathcal{H}_\infty$, μ-synthesis and QFT controllers have not been successfully implemented and hence are not considered below.

1) Frequency Domain Response: Figure 7(a) shows that, except for LQR-LQG, the simulated closed loop frequency responses of the implemented controllers have good tracking properties for sinusoidal references of frequencies up to 50rad/s (within a bound of ± 0.01 for T). After the implementation of the discretized controllers on the MPS, it is observed that the tracking characteristics hold at the low frequencies but at intermediate and high frequencies there is an increase in the magnitude. In particular, there is a resonance at about 90Hz in all the frequency responses, the same resonance that appeared during the model validation. The discrepancy at high frequencies is believed to be due to high frequency dynamics not considered in the analytical model (this difference was believed to have been accounted for in the uncertainty models employed in the $\mathcal{H}_\infty$, μ-synthesis and QFT designs). The requirement of a rise time of 0.1s for a step response makes the controlled dynamics important under 100Hz. Hence, even *without* a good match between simulated and experimental responses at high frequencies, it was possible to implement the lead-lag, LQG-LQR, LQG-LTR and SISO $\mathcal{H}_\infty$ controllers. The MIMO $\mathcal{H}_\infty$, μ-synthesis and QFT designs, which considered the modeled uncertainty, were unstable in implementation.

[5]Implemented considering decentralized decoupled SISO $\mathcal{H}_\infty$ designs.

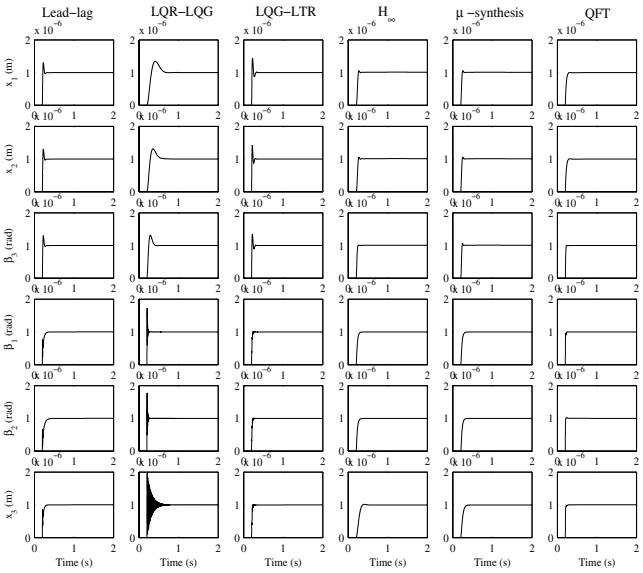

Fig. 6. Numerical simulation results, step response, various controllers.

From the control effort plots, Fig. 7(b), the controller $\mathcal{H}_\infty$ requires less energy despite having equal or better tracking performance than the controllers lead-lag and LQG-LTR.

2) Time Domain Response: From Fig. 7(c)-(d), there is a fairly close match between the numerical simulation and the experimental results. However, there is a slight difference in transient (damping) of the responses. This difference may be a consequence of high frequency unmodeled dynamics as is evident from the frequency plots. The experimental responses show residual motions not apparent in simulations. The residual motions have envelopes of approximately 0.05μm in all the cases except for the LQR-LQG controller, which shows oscillations with amplitudes of 0.4μm and 0.15μm at about 2 and 1000Hz. The LQG-LTR and lead-lag controllers appear to achieve quicker responses at the expense of higher values of control input.

V. CONCLUSIONS AND FUTURE WORK

A. Conclusions

The present study considered the control of a MPS using a variety of control methods. The MPS employs three novel permanent-magnet linear motors. The employed SISO and MIMO control approaches assumed linearized models that are uncoupled for certain axes, with the actual system's dynamic being nonlinear and coupled. The effectiveness of the control methods was compared analytically, with consideration given to the difference in how the problem is posed and solved for each methodology. The $\mathcal{H}_\infty$ norm and μ scalar of frequency weighted functions facilitated

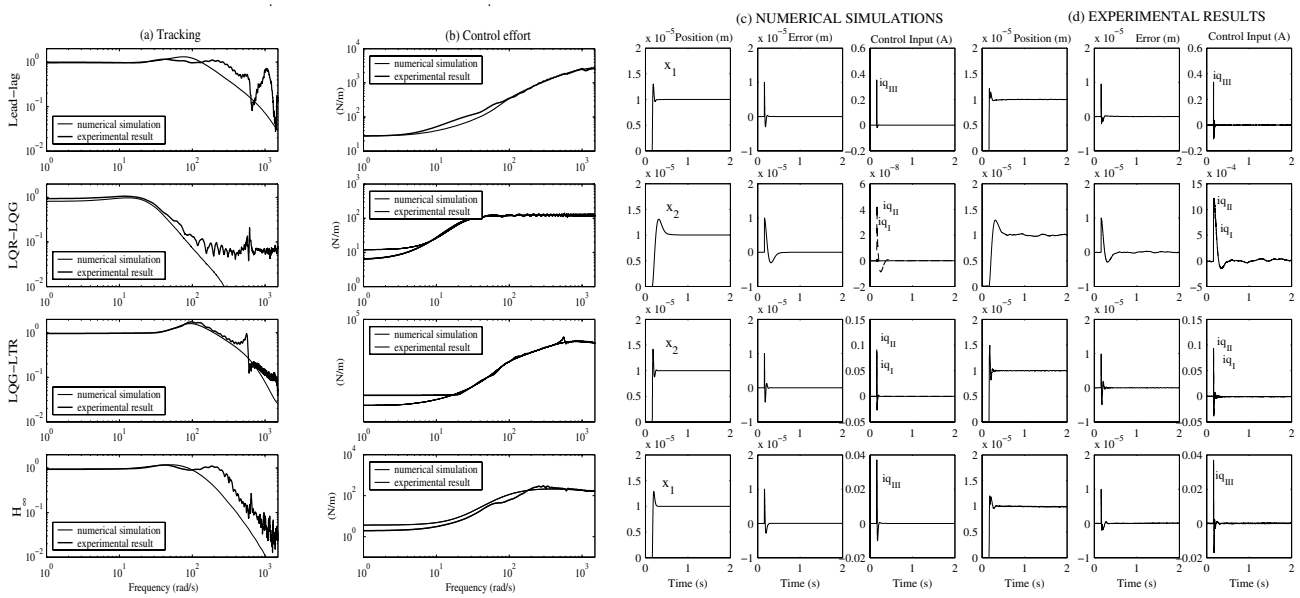

Fig. 7. Numerical simulation and experimental results for step references in x_1 and x_2. Frequency response: (a) Tracking and (b) Control effort. (c)-(d) Time response: position, position error and control current.

the comparison. Stability robustness was incorporated in the analysis by considering diagonal perturbations. This analysis was performed under the implicit assumption that the uncertainty model considered captures the behavior of the experimental system. The results of the analysis showed that the $\mathcal{H}_\infty$ and μ-synthesis controllers satisfied the RS condition with acceptable performance over the uncertainty range. The remaining controllers violated the RS condition by factors of up to 80, with LQR-LQG having the best RS properties and QFT having the best NP of all the controllers.

In implementation, the lead-lag, LQR-LQG, LQG-LTR and SISO $\mathcal{H}_\infty$ controllers successfully controlled the MPS with positioning capability. Despite the fact that the $\mathcal{H}_\infty$ and μ-synthesis controllers satisfied the RS condition, and were the only ones, they failed in implementation along with the QFT controller. Whilst unexpected, this indicates that the uncertain model failed to capture the dynamics of the real system. Notably, controllers that violated the RS condition were successfully implemented and provided precise response at the operating condition. For these controllers, the frequency and time domain simulations and experimental results confirmed the existence of a mismatch between the analytical model and the real system.

B. Future Work

The experimental results indicated that the present nominal model with associated uncertainty is inadequate for reliable controller design. Similar work [8] confirms the importance of both an accurate nominal model and uncertainty description. However, whilst seemingly feasible in [8], simply increasing the level of uncertainty is clearly not sufficient, indicating that the directionality of the uncertainty may have to be taken into account. Subsequently, further work aims to improve the uncertainty description using methods such as [9] and investigate the presence of unmodeled dominant dynamics that may have contributed to the multivariable design failures. The redesign and implementation of the considered controllers would then be undertaken along with further investigation into the action of each controller (maximum range of operation and position resolution of the controlled MPS).

VI. ACKNOWLEDGMENTS

The authors gratefully acknowledge the contribution of Dr. Won-jong Kim, Tiejun Hu and reviewers' comments.

REFERENCES

[1] M. Athans, *A Tutorial on the LQG/LTR Method*, Laboratory for Information and Decision Systems, M.I.T., Cambridge, MA, March 1986.
[2] N. Bhat, *ATP Project Report*, June 2003.
[3] G. Balas, J. Doyle, K. Glover, A. Packard and R. Smitht, *μ-Analysis and Synthesis Toolbox*, User's Guide, 1993.
[4] B.D.O. Anderson and J.B. Moore, *Linear Optimal Control*, Prentice Hall, New Jersey, NJ, 1971.
[5] G. Franklin, A. Emami-Naeini, J. Powell *Feedback Control of Dynamic Systems,*, Addison-Wesley Longman Publishing Co., Inc., Boston, MA, 1994.
[6] W.J. Kim, *High Precision Planar Magnetic Levitation*, Ph.D. Thesis, Massachusetts Institute of Technology, Cambridge, MA, June 1997.
[7] W.J. Kim, D.L. Trumper, J.H. Lang, *Modeling and Vector Control of Planar Magnetic Levitator*, IEEE Transactions on Industry Applications, vol. 34, no. 6, p. 1254-1262, December 1998.
[8] K.B. Lim and D.E. Cox, *Experimental Robust Control Studies on an Unstable Magnetic Suspension System*, American Control Conference, vol. 3, 29 June-01 July 1994.
[9] K.B. Lim, D.E. Cox, G.J. Balas and J-N. Juang, *Validation of an Experimentally Derived Uncertainty Model*, 35th AIAA Aerospace Sciences Meeting & Exhibit, Reno, NV, AIAA 97-0244, January 6-9, 1997.
[10] U. Forssell, L. Ljung, *Closed-loop identification revisited*, Automatica, vol. 35, p. 1215-1241, 1999.
[11] O. Yaniv *Quantitative Feedback Design of Linear and Nonlinear Control Systems*, Kluwer Academic Pub., The Netherlands, 1999.
[12] K. Zhou, J. Doyle, K. Glover *Robust and Optimal Control*, Prentice Hall, New Jersey, NJ, 1996.